NANO LETTERS
Letter
Cite This: Nano Lett. 2018, 18, 1592−1599
pubs.acs.org/NanoLett

# Delocalized Impurity Phonon Induced Electron−Hole Recombination in Doped Semiconductors

Lili Zhang,[†,∇,○] Qijing Zheng,[†,∇,○] Yu Xie,[‡] Zhenggang Lan,[‡] Oleg V. Prezhdo,[§] Wissam A. Saidi,[∥] and Jin Zhao*[,†,⊥,#]

[†]ICQD/Hefei National Laboratory for Physical Sciences at Microscale and Key Laboratory of Strongly-Coupled Quantum Matter Physics, Chinese Academy of Sciences, Hefei, Anhui 230026, China

[‡]Key Laboratory of Biobased Materials, Qingdao Institute of Bioenergy and Bioprocess Technology, Chinese Academy of Sciences, Qingdao, Shandong 266101, China

[§]Departments of Chemistry, and Physics and Astronomy, University of Southern California, Los Angeles, California 90089, United States

[∥]Department of Mechanical Engineering and Materials Science, University of Pittsburgh, Pittsburgh, Pennsylvania 15261, United States

[⊥]Department of Physics and Astronomy, University of Pittsburgh, Pittsburgh, Pennsylvania 15260, United States

[#]Synergetic Innovation Center of Quantum Information & Quantum Physics and [∇]Department of Physics, University of Science and Technology of China, Hefei, Anhui 230026, China

*Supporting Information*

**ABSTRACT:** Semiconductor doping is often proposed as an effective route to improving the solar energy conversion efficiency by engineering the band gap; however, it may also introduce electron−hole (e−h) recombination centers, where the determining element for e−h recombination is still unclear. Taking doped $TiO_2$ as a prototype system and by using time domain ab initio nonadiabatic molecular dynamics, we find that the localization of impurity-phonon modes (IPMs) is the key parameter to determine the e−h recombination time scale. Noncompensated charge doping introduces delocalized impurity-phonon modes that induce ultrafast e−h recombination within several picoseconds. However, the recombination can be largely suppressed using charge-compensated light-mass dopants due to the localization of their IPMs. For different doping systems, the e−h recombination time is shown to depend exponentially on the IPM localization. We propose that the observation that delocalized IPMs can induce fast e−h recombination is broadly applicable and can be used in the design and synthesis of functional semiconductors with optimal dopant control.

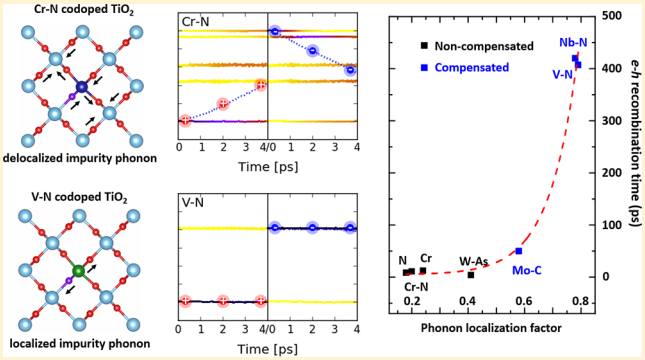


**KEYWORDS:** *Semiconductor doping, electron−hole recombination, nonadiabaic molecular dynamics, impurity-phonon mode*

Developing advanced functional materials for clean and sustainable energy applications is an extremely active research area. Significant efforts have been devoted to search for environmentally friendly materials for solar energy conversion, in which improving the efficiency by functional material design is of great importance.

The solar-energy conversion efficiency of wide band gap semiconductors is significantly limited due to their large intrinsic band gaps, which makes them absorbers only in the ultraviolet portion of the solar spectrum.[1−18] Cation and anion doping or co-doping is a well-known technique to optimize the band gap of semiconductors. For example, numerous attempts have been made to engineer the band gap of $TiO_2$, which is a promising solar energy conversion material, using different doping schemes,[5,10−32] among which the n-p co-doping concepts are proposed to improve the thermodynamic solubility over monodoping.[18,24,25,31,32] However, it is well-known that doping can induce electron−hole (e−h) recombination centers, which decrease the solar energy conversion efficiency.[9,33−37] In contrast to the well-established concept that the band gap is the critical factor for light-absorption properties,[24−26,38−45] it is still unclear what is the determining factor for the e−h recombination induced by the impurity states in doped semiconductors.

The development of time-resolved nonadiabatic molecular dynamics (NAMD) makes it possible to investigate the e−h recombination rates using state-of-the-art ab initio calcula-

Received: September 13, 2017
Revised: January 31, 2018
Published: February 2, 2018






DOI: 10.1021/acs.nanolett.7b03933
Nano Lett. 2018, 18, 1592−1599

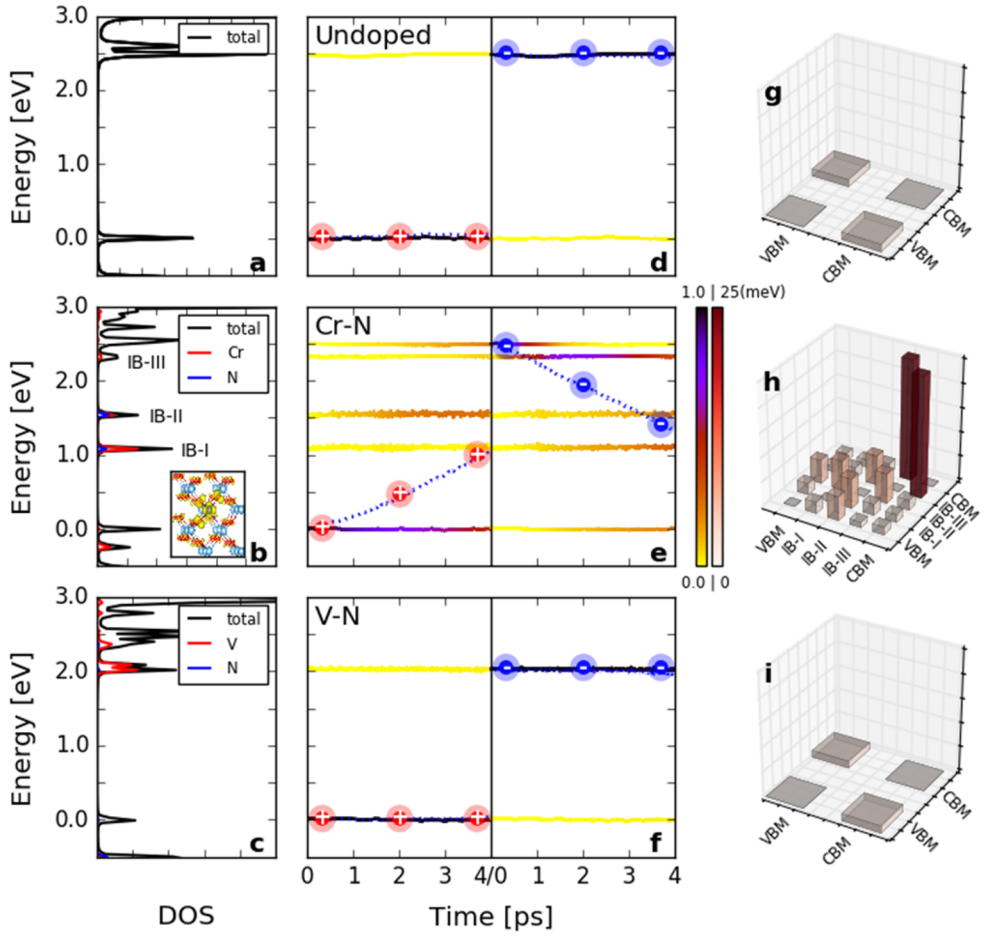


**Figure 1.** Electronic structures and the time-dependent electron/hole (e/h) dynamics in undoped, Cr−N- and V−N-doped $TiO_2$. (a−c) The total and partial DOS. (d−f) The averaged time-dependent e/h energy relaxation at 300 K. The color strip indicates the e/h distribution on different energy states, and the dashed line represents the averaged e/h energy. The energy reference is the average VBM energy. (g−i) The averaged NAC elements in undoped and Cr−N- and V−N-doped $TiO_2$ at 300 K. The inset in panel b shows the spatial distribution of the excess charge induced by Cr−N codoping, in which the Ti, O, Cr, and N atoms are marked by large light blue, small red, large deep blue, and small purple balls, respectively.

tions.[46] Taking rutile $TiO_2$ as a prototype system, we use NAMD to investigate the e−h recombination rates with different doping schemes. We find that charged doping centers, which are formed in monodoped and non-compensated n-p co-doped $TiO_2$, introduce delocalized impurity phonon modes (IPMs). The excitation of these IPMs induces ultrafast e−h recombination through the electron−phonon (e−p) interaction. In such systems, e−h recombination time scale decreases from nanosecond (ns) magnitude for the undoped $TiO_2$ to a few picoseconds (ps). Such ultrafast e−h recombination can be successfully suppressed if their IPMs are significantly localized, which can be realized by charge-compensated co-doping with light elements. Thus, the e−h recombination time can be kept as long in the nanosecond scale. Furthermore, we show that the e−h recombination time scale depends exponentially on the localization of IPMs, making it the determining element for solar efficiency in doped semiconductors. These findings establish that the excitation of delocalized IPMs induces fast e−h recombination, which is a powerful guiding principle in future design of functional materials for solar-energy conversion.

The ab initio NAMD simulations are carried out using homemade Hefei-NAMD code,[47] which augments the Vienna ab initio simulation package (VASP)[48−50] with the NAMD capabilities within time domain density functional theory (TDDFT) similar to refs 51−53 The generalized gradient approximation functional of PBE[54] and the projector augmented wave (PAW)[55] approximation for the core electrons are used. We use a $2 \times 2 \times 3$ supercell containing 24 $TiO_2$ units to model the bulk rutile $TiO_2$. To overcome the well-known self-interaction error in DFT, we use the GGA + $U$ method to treat the 3$d$ electrons of the transition metals ($U$ = 6 eV for Ti; $U$ = 3 eV for V Cr, W; and $U$ = 2.5 eV for Mo). After geometry optimization, we use velocity rescaling to bring the temperature of the system to either 100 or 300 K. A 8 ps microcanonical ab initio molecular dynamics trajectory is then generated using a 1 fs time step. The NAMD results are obtained by averaging over 100 different initial configurations selected from the MD trajectory based on the classical path approximation.[56] For each chosen structure, we sample $2 \times 10^4$ trajectories for the last 5 ps.

Regular NAMD simulation can emulate the dynamics of excited charge carriers at a certain temperature, wherein the excitations of many different phonon modes are included. To understand how the carrier dynamics depend on a spectific phonon mode, the frozen phonon NAMD is performed. This is done by choosing a specific phonon mode, and generating the corresponding atomic trajectory in which the vibrational amptitude is determined by the average kinetic energy of this phonon mode as $\langle K \rangle = 3N \cdot \frac{1}{2} K_B T$ ($N$ is the number of atoms,



DOI: 10.1021/acs.nanolett.7b03933
Nano Lett. 2018, 18, 1592−1599

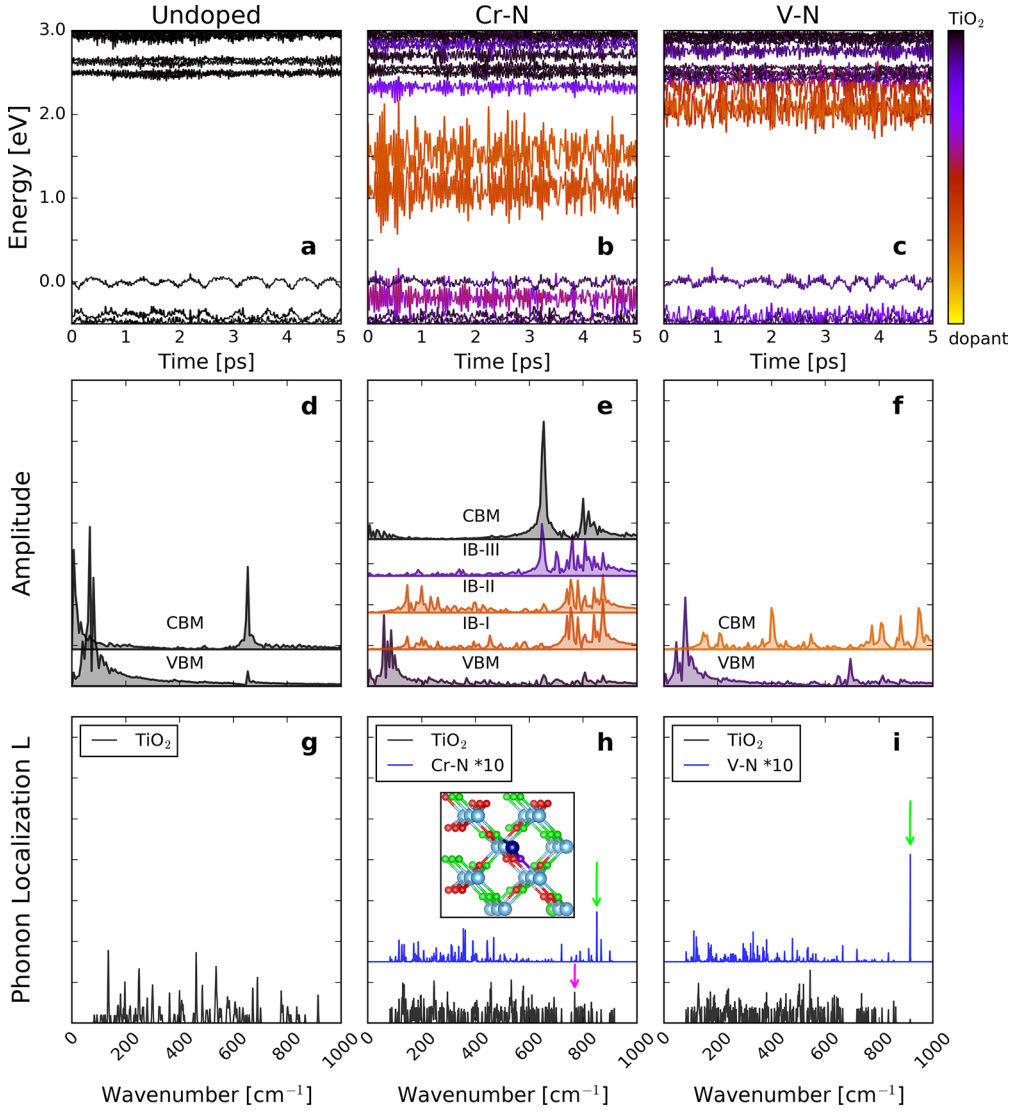


**Figure 2.** Time evolutions of the state energies near VBM and CBM for undoped and Cr−N- and V−N-co-doped $TiO_2$ (a−c) and their FT spectra (d−f) at 300 K. The spatial localization of phonon modes (g−i). The inset in panel h shows by green color the atoms that vibrate coherently with Cr−N. In panels h and i, the green arrows indicate the major IPMs in Cr−N- and V−N-doped $TiO_2$. The color map indicates the orbital localization (black on $TiO_2$ and yellow on dopant). A typical $TiO_2$ bulk phonon mode in Cr−N-doped $TiO_2$ is marked by a purple arrow.

and $T$ is the temperature). In this work, we use $T$ = 100 K to generate a reasonable vibrational amplitude. The NAMD results are obtained by averaging $2 \times 10^4$ electronic trajectories. Molinari et al. have used a similar idea for analyzing the role of phonons in ultrafast dynamics of polaron pairs in conjugated polymers.[57]

The e−h recombination time is estimated as the time at which the electron and hole both reach one of the intermediate bands (IBs), which are located in the band gap. For the systems without IBs in the band gap, it is estimated as the time scale when either the electron or hole reaches the VBM or CBM, respectively.

We start with n-p co-doped $TiO_2$, which is a potential candidate to improve the thermodynamic stability compared to monodoping.[24,25] Noncompensated Cr−N and compensated V−N co-doping are chosen for contrast. Before presenting the results based on NAMD calculations, it is instructive to establish the electronic structures of n-p co-doped $TiO_2$. Figure 1a−c shows the density of states (DOS) of optimized undoped as well as Cr−N- and V−N-co-doped $TiO_2$. Similar to previous results,[24,25] Cr−N co-doping introduces three IBs, two localized bands (labeled as IB-I and IB-II) mostly contributed by Cr−N in the middle of the band gap, and one hybridized band (IB-III) contributed by both $TiO_2$ and Cr−N near the CBM. As a net n-type noncompensated co-doping, one excess electron is introduced by Cr−N. In contrast, as compensated co-doping, V−N does not introduce IBs in the band gap; instead, it narrows the band gap to around 2.0 eV due to the downward and upward shifts of the CBM and VBM, respectively. As shown in Figure 1c, CBM is mostly contributed by the V 3*d* orbital, and VBM is hybridized by O and N 2*p* orbitals.

We choose CBM and VBM as the initial states for electron and hole excitations. The e−h recombination in Cr−N- and V−N-co-doped $TiO_2$ exhibits distinctly different behavior at 300 K. For undoped and V−N-co-doped $TiO_2$, as shown in Figure 1d,f, within the 4 ps of NAMD, the e−h recombination can be hardly seen. This suggests that the e−h recombination time scale is much longer than the picosecond magnitude, which cannot be accurately obtained from these NAMD simulations.



DOI: 10.1021/acs.nanolett.7b03933
*Nano Lett.* 2018, 18, 1592−1599

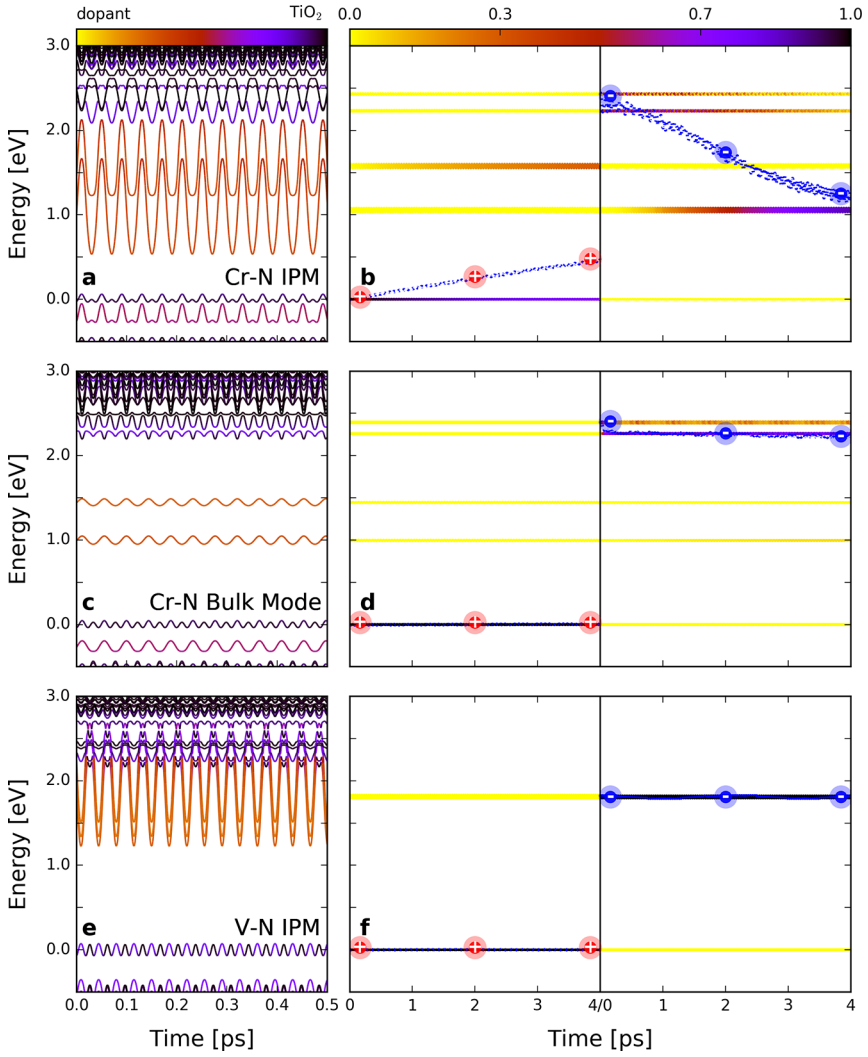


**Figure 3.** Frozen phonon NAMD results for time evolutions of the energy states near VBM and CBM and the averaged time-dependent e/h energy relaxation for Cr−N- and V−N-co-doped $TiO_2$. (a,b) IPM for Cr−N-doped $TiO_2$. (c,d) A single bulk mode for Cr−N-doped $TiO_2$. (e,f) IPM for V−N-doped $TiO_2$. The energy reference is the average VBM energy. The color map in a indicates the orbital localization (black on $TiO_2$ and yellow on dopant). The color map in b indicates the e/h distribution on different energy states.

We can roughly estimate the e−h recombination time to be around 0.5 ns by fitting with an exponential decay function.[58] In previous studies, the e−h lifetime varies in the range from picoseconds to microseconds,[59−64] which can be attributed to the different experimental techniques and quality of the sample. Our result is consistent with recent experimental measurements.[59,60] There is also one previous theoretical investigation based on GW approximation, in which the e−h lifetime was estimated to around 30−40 fs, which we believe is too short for the charge-carrier lifetimes of semiconductors.[65] For Cr−N-co-doped $TiO_2$, as shown in Figure 1e, the e−h recombination takes place in about 4−5 ps in distinct contrast to undoped and V−N-co-doped systems in which the lifetimes are in ns range. For a Cr−N-co-doped system, the two localized IBs in the band gap are clearly shown to be the e−h recombination centers by trapping the charge carriers.

In NAMD simulations, the hopping probability of excited e/h between different energy states depends on the nonadiabatic coupling (NAC) elements, which can be written as:

$$d_{jk} = \left\langle \varphi_j \left| \frac{\partial}{\partial t} \right| \varphi_k \right\rangle = \frac{\langle \varphi_j | \nabla_R H | \varphi_k \rangle}{\epsilon_k - \epsilon_j} \dot{R} \quad (1)$$

In eq 1, $H$ is the Kohn−Sham Hamiltonian; $\varphi_j$, $\varphi_k$, $\epsilon_j$, and $\epsilon_k$ are the corresponding wave functions and eigenvalues for electronic states j and k; R is the position of the nuclei; and $\dot{R}$ is velocity of the nuclei.[66] Figure 1g−i shows the averaged NAC elements of undoped and Cr−N- and V−N-co-doped $TiO_2$ at 300 K. In Cr−N-co-doped $TiO_2$, the largest NAC is 25 meV, which is 16 times larger than the NAC between CBM and VBM in undoped and V−N-co-doped $TiO_2$ (around 1.5 meV). From eq 1, one can see that the NAC elements show strong dependence on the energy difference $\epsilon_k$-$\epsilon_j$ of the interacting states, the e−p coupling term $\langle \varphi_j | \nabla_R H | \varphi_k \rangle$ and the nuclear velocity $\dot{R}$. Comparing V−N to Cr−N co-doping, at zero temperature, the energy difference between the VBM and CBM in a V−N system (around 2.0 eV) is approximately double of that between VBM or CBM and IBs in Cr−N-co-doped $TiO_2$ (around 1.0 eV). The energy difference between the electronic states is one reason for inducing different NAC. However, this alone does not explain the distinct differences between Cr−N-



DOI: 10.1021/acs.nanolett.7b03933
Nano Lett. 2018, 18, 1592−1599

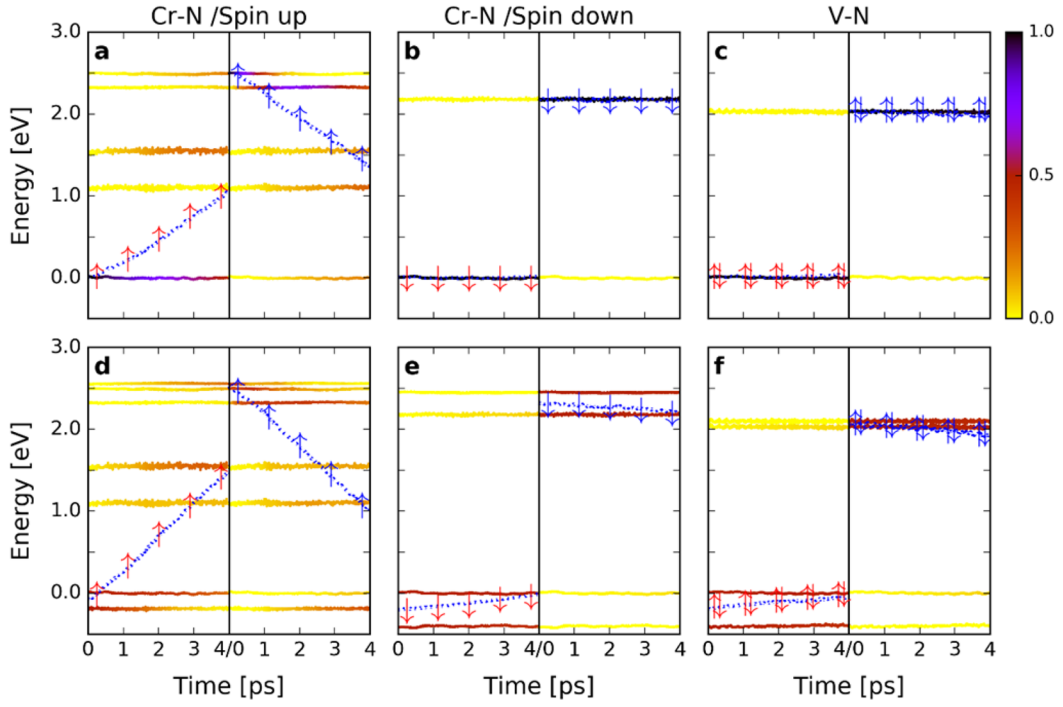


**Figure 4.** Spin-polarized time-dependent e/h energy relaxation for Cr−N- and V−N-co-doped $TiO_2$ with $n$ = 2.67 e/nm$^3$ (a−c) and $n$ = 5.34 e/nm$^3$ (d−f).

and V−N-co-doped systems. The other two factors $\langle\varphi_j|\nabla_R H|\varphi_k\rangle$ and $\dot{R}$ are both strongly dependent on the phonon excitation and e−p coupling, which are crucial for the NAMD dynamics.

Doping impurities in semiconductors can induce IPMs that may scatter and couple with bulk phonon modes,[67−69] which usually have strong e−p coupling with impurity induced electronic states. IPMs can be determined by computing the phonon spatial localization (labeled as $L$ in Figure 2g−i) of all of the normal modes in Cr−N- and V−N-co-doped $TiO_2$ and project them onto the dopants, similar to ref 69. As shown in Figure 2h, clearly, Cr−N has coupling with $TiO_2$ bulk modes within a wide range, indicating that they scatter with bulk phonon modes that have different frequencies and momentum. In addition, Cr−N contributes one major IPM around 820 cm$^{-1}$, which is indicated by the green arrow. Figure 2i shows that V−N has relatively weaker scattering with the bulk phonon modes, and the major IPM is located at 920 cm$^{-1}$. IPMs of both V−N and Cr−N are stretching modes between the two doping atoms. However, distinct differences can be found by looking into projected spatial localization ($L_{V-N}$ and $L_{Cr-N}$) and the atomic displacements of these IPMs. For V−N, the major IPM is a localized mode, which has a negligible coupling with neighboring Ti and O atoms. In contrast, the major Cr−N IPM shows strong coupling with $TiO_2$ bulk. As shown in the inset of Figure 2h, where the Ti and O atoms involved in Cr−N IPM are marked using a green color, about half of the atoms in the supercell vibrate coherently with Cr and N. Such a significant delocalized character originates from the excess charge induced by Cr−N codoping, which can be confirmed by inspecting the spatial distribution of the electron density shown in the inset of Figure 1b. These results show that the excess charge is distributed not only on doped Cr−N atoms but also on neighboring Ti and O atoms, which plays a role in the strong coherent vibration of Cr−N with the Ti and O atoms.

The e−p coupling of IPMs with the electronic states that are involved in e−h recombination can be qualitatively understood from the time-dependent energy evolution of the electronic states and their Fourier transform (FT) spectra (Figure 2a−f). The strength of the electronic-state energy fluctuations amplitude is directly correlated with the strength of e−p coupling. Furthermore, the FT spectra reveal the dominant phonon modes involved in the NAMD. Figure 2b shows that there are strong energy fluctuations for localized IB-I and IB-II in Cr−N co-doped $TiO_2$, which are as large as 1.2 eV at 300 K. Compared to Cr−N, in V−N-co-doped $TiO_2$ (Figure 2c), the CBM, which is contributed mostly by V 3$d$, has a fluctuation amptitude around 0.5 eV, and the VBM, which is hybridized by N and O, has a fluctuation amptitude of 0.2 eV, similar to the undoped $TiO_2$ (Figure 2a). The large extent of energy fluctuations in Cr−N-doped $TiO_2$ indicates that there is a strong e−p coupling for the IBs. As seen from the FT spectra shown in Figure 2e in Cr−N co-doped $TiO_2$, the major phonon peaks couple with the IBs localized around 820 cm$^{-1}$, corresponding to the Cr−N stretching IPM. It suggests a strong e−p coupling of the IBs with the Cr−N stretching IPMs. Moreover, CBM and VBM also couple with Cr−N stretching IPM. This is because the Cr−N stretching IPM has a delocalized character involving many $TiO_2$ bulk atoms. In contrast, in V−N-doped $TiO_2$ (Figure 2f), only the V 3$d$ contributed CBM shows coupling with the localized V−N stretching IPM. Our results show that in Cr−N doped $TiO_2$, all of the electronic states involved in the e−h recombination couple with the IPM that has a delocalized character. Therefore, once the IPM is excited, the coherent vibration involves around half of the atoms in one supercell, which significantly enhances the nuclear velocity and the NAC e−p coupling term. Meanwhile, the energy difference term $\epsilon_k - \epsilon_j$ is also reduced due to the strong energy fluctuations of IBs. Hence, we propose


DOI: 10.1021/acs.nanolett.7b03933
Nano Lett. 2018, 18, 1592−1599

that the large NACs, which induce fast e−h recombination, mostly originate from the excitation of the delocalized IPMs.

We verify the important role of IPMs using frozen phonon NAMD, in which we can choose one specific phonon mode and investigate the excited carrier dynamics coupled with it. We select the IPMs of Cr−N and V−N doped $TiO_2$ and a typical bulk mode of Cr−N doped $TiO_2$ and compare the dynamics of excited carriers. As shown in Figure 3a, in Cr−N doped $TiO_2$, when the IPM is excited, the energies of IB-I and IB-II show distinct oscillations because of the strong e−p coupling. IB-III and CBM also exhibit significant coupling with the Cr−N IPM. In this case, the e−h recombines at around 5 ps, as shown in Figure 3b. In contrast, if only a bulk phonon mode (indicated by the purple arrow in Figure 2h) is excited, as shown in Figure 3c,d, the e−h recombination is significantly suppressed. In such a case, the e−h recombination time scale can be as long as nanoseconds. Contrarily, in V−N-doped $TiO_2$, the excitation of localized IPM only induces the energy oscillation of CBM, and it does induce a slow e−h recombination in the nanosecond scale, as shown in Figure 3e,f. The phonon effects are further confirmed by NAMD calculations at 100 K. With lower temperature, the phonon occupation is reduced and the e−h recombination is slower. (See details in the Supporting Information.)

The discussion above is based on the single excitation, where only one electron or hole is generated on CBM or VBM. In this case the charge density can be estimated as $n$ = 1.33 e/nm$^3$. If we double the charge density ($n$ = 2.67 e/nm$^3$), suggesting that CBM or VBM is fully occupied by two electrons or holes with different spin, the carrier dynamics in V−N-doped $TiO_2$ will not change because it is a spin-unpolarized system in which the dynamics of spin-up and spin-down carriers are the same. Yet it is quite different for Cr−N doped $TiO_2$, which is a spin-polarized system, and the defect states are all spin-up states. It is very interesting to find that for the spin down electrons and holes, the e−h recombination is very slow because the defect states are in the spin up channel. As shown in Figure 4b, within 4 ps, such e−h recombination is hardly seen. Therefore, the e−h recombination time scale can be estimated to be on a nanosecond scale, which is comparable to V−N-doped $TiO_2$.

We also investigate the case in which there are four electrons and holes excited in one supercell, which can be converted to a charge density of $n$ = 5.34 e/nm$^3$ with CBM/VBM and CBM + 1/VBM − 1 occupied. In this case, the e−h recombination in Cr−N doped $TiO_2$ still takes place within 5 ps for spin-up carriers. For spin-down carriers, one can observe the e/h relaxation from CBM + 1/VBM − 1 to CBM/VBM is within 4 ps. Yet the e−h recombination is still hardly seen, which shows similar character with V−N-doped $TiO_2$. The results prove that the fast e−h recombination in Cr−N-doped $TiO_2$ is spin-polarized. This suggests that the remained electrons and holes that have ns magnitude lifetime are also spin-polarized, which makes Cr−N-doped $TiO_2$ of potential interest for applications in spintronic devices.

We propose that the fast e−h recombination induced by delocalized IPMs applies to different kinds of doping systems. To confirm this, we investigate mono Cr and N doping, another noncompensated co-doping by W and As, which are heavier elements in the same group with Cr and N and another two compensated co-doped systems by Mo−C and Nb−N. To quantify the correlation between the IPM localization with the e−h recombination time, we define $F_{LOC} = L_{impurity}/L_{total}$ as a measure of the localization level of IPMs, in which $L_{total}$ and $L_{impurity}$ are the spatial localization of the IPM and the projection onto the impurity atoms. A larger $F_{LOC}$ suggests a more-localized IPM. As shown in Figure 5, for all of the seven

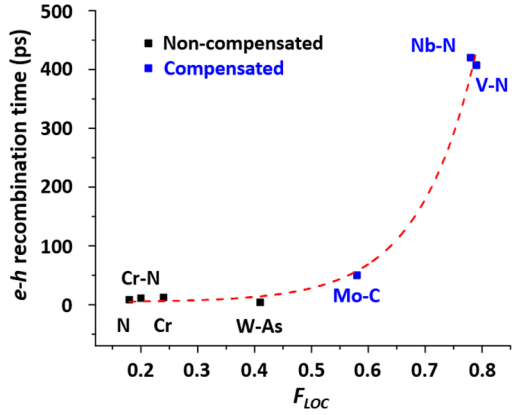


**Figure 5.** e−h recombination time in different doped $TiO_2$. The fitting exponential correlation is shown with dashed lines.

investigated doped systems, the e−h recombination time shows an exponential dependence on $F_{LOC}$ at 300 K, suggesting that $F_{LOC}$ is a key parameter determining the e−h recombination time. $F_{LOC}$ is affected by several factors. First, it is strongly affected by the compensation of the dopants. It can be seen that all the mono- and noncompensated impurities have delocalized IPMs. This is because the excess charge in non-compensated doping systems induces coupling with $TiO_2$ atoms around the doping sites. The IPMs can be localized when the dopants are compensated and the e−h recombination time increases. Second, the mass of the dopants is another factor. For compensated doping, comparing Mo−C to V−N, introducing the heavier element Mo splits the stretching IPM into two peaks. The higher one at 1100 cm$^{-1}$, which is mostly associated with C, is strongly localized. The lower one at 100 cm$^{-1}$ associated with Mo is a delocalized IPM that significantly couples with acoustic bulk phonons in $TiO_2$, which makes the e−h recombination in Mo−C not as slow as in V−N. The effects of mass can be also seen in noncompensated doping. Comparing W−As to Cr−N, the IPMs in W−As-doped $TiO_2$ are softer due to larger mass and moves from 820 cm$^{-1}$ for Cr−N to around 80 cm$^{-1}$ for W−As, which make them easier to excite and couple with the acoustic modes in $TiO_2$ (see the Supporting Information for more details). Therefore, the e−h recombination time is only 1.2 ps at 300 K for W−As. We propose that the compensated n-p codoping with light dopants such as V−N, which has localized IPMs, is the ideal doping scheme to improve the light absorption and at the same time, avoids the formation of e−h recombination centers. This is partially substantiated by experimental results, which report high visible-light photocatalytic activity in V−N co-doped $TiO_2$.[22,70−75] For non-compensated co-doping or monodoping systems, e−h recombination is usually fast. However, if the defect states are spin-polarized, the fast e−h recombination will be spin-polarized too, which makes them attractive for spintronic devices.

In summary, our results prove that the spatial localization of IPMs, which can be estimated by a localization factor $F_{LOC}$, plays a crucial role in the e−h recombination process. Delocalized IPMs that involve many atoms induce fast e−h recombination through e−p coupling, whereas the localized



DOI: 10.1021/acs.nanolett.7b03933
Nano Lett. 2018, 18, 1592−1599

IPMs do not contribute to the e−h recombination. The exponential correlation between the e−h recombination time with localization factor $F_{LOC}$ suggests that, similar to the band gap being a critical factor for the light absorption efficiency, the localization of IPMs is the determining criterion for the e−h recombination time, which is a guiding principle for the design and synthesis of advanced functional semiconductors with optimal dopants control for solar-energy conversion.

## ■ ASSOCIATED CONTENT

### Supporting Information

The Supporting Information is available free of charge on the ACS Publications website at DOI: 10.1021/acs.nanolett.7b03933.

Additional details and figures regarding NAMD investigations on the e−h recombination of undoped and Cr−N- and V−N-doped $TiO_2$ at 100 K; calculations of normal vibration modes of Cr- and N-monodoped and Mo−C- and W−As-co-doped $TiO_2$; NAMD investigations on the e−h recombination of Cr- and N-monodoped and Mo−C- and W−As-co-doped $TiO_2$ effects on impurity concentration, K-point sampling, and electric field. (PDF)

## ■ AUTHOR INFORMATION


### Corresponding Author

*E-mail: zhaojin@ustc.edu.cn. Phone: +86-551-63602832.

### ORCID

Yu Xie: 0000-0001-8925-6958

Oleg V. Prezhdo: 0000-0002-5140-7500

Wissam A. Saidi: 0000-0001-6714-4832

Jin Zhao: 0000-0003-1346-5280

### Author Contributions

○L.Z. and Q.Z. contributed equally to this work.


### Notes

The authors declare no competing financial interest.

## ■ ACKNOWLEDGMENTS

J.Z. acknowledges the support of the Ministry of Science and Technology of China, grant nos. 2016YFA0200604 and 2017YFA0204904; National Natural Science Foundation of China, grant nos. 11620101003, 21421063; the Fundamental Research Funds for the Central Universities, grant no. WK3510000005; and the support of the U.S. National Science Foundation, grant no. CHE-1213189. Q.Z. acknowledges the support of the National Natural Science Foundation of China, grant no. 11704363. Z.L. acknowledges the support of the National Natural Science Foundation of China, grant no. 21673266, and the support of the Natural Science Foundation of Shandong Province for Distinguished Young Scholars (JQ201504). Y.X. acknowledges the support of the National Natural Science Foundation of China, grant no. 21503248. W.A.S. acknowledges a start-up grant from the department of Mechanical Engineering and Materials Science at the University of Pittsburgh. O.V.P. acknowledges the support of the US National Science Foundation, grant no. CHE-1565704. Calculations were performed in part at Environmental Molecular Sciences Laboratory at the PNNL, a user facility sponsored by the DOE Office of Biological and Environmental Research; the Supercomputing Center at USTC; the Argonne Leadership Computing Facility, which is a DOE Office of Science User Facility supported under contract no. DE-AC02-06CH11357; and the Pittsburgh Supercomputing Center.

## ■ REFERENCES


(1) Fujishima, A.; Honda, K. *Nature* **1972**, *238*, 37−38.
(2) Fujishima, A.; Zhang, X.; Tryk, D. A. *Surf. Sci. Rep.* **2008**, *63*, 515−582.
(3) Thompson, T. L.; Yates, J. T., Jr. *Chem. Rev.* **2006**, *106*, 4428−4453.
(4) Grätzel, M. *Nature* **2001**, *414*, 338−344.
(5) Asahi, R.; Morikawa, T.; Ohwaki, T.; Aoki, K.; Taga, Y. *Science* **2001**, *293*, 269−271.
(6) Henderson, M. A. *Surf. Sci. Rep.* **2011**, *66*, 185−297.
(7) Diebold, U. *Surf. Sci. Rep.* **2003**, *48*, 53−229.
(8) Hoffmann, M. R.; Martin, S. T.; Choi, W.; Bahnemann, D. W. *Chem. Rev.* **1995**, *95*, 69−96.
(9) Ozgur, U.; Alivov, Y. I.; Liu, C.; Teke, A.; Reshchikov, M. A.; Dogan, S.; Avrutin, V.; Cho, S. J.; Morkoc, H. *J. Appl. Phys.* **2005**, *98*, 041301.
(10) Van de Walle, C. G.; Neugebauer, J. *J. Appl. Phys.* **2004**, *95*, 3851−3879.
(11) Ferrighi, L.; Datteo, M.; Fazio, G.; Di Valentin, C. *J. Am. Chem. Soc.* **2016**, *138*, 7365−7376.
(12) Jimenez, J. M.; Bourret, G. R.; Berger, T.; McKenna, K. P. *J. Am. Chem. Soc.* **2016**, *138*, 15956−15964.
(13) Wang, Z. Q.; Wen, B.; Hao, Q. Q.; Liu, L. M.; Zhou, C. Y.; Mao, X. C.; Lang, X. F.; Yin, W. J.; Dai, D. X.; Selloni, A.; Yang, X. M. *J. Am. Chem. Soc.* **2015**, *137*, 9146−9152.
(14) Dahlman, C. J.; Tan, Y. Z.; Marcus, M. A.; Milliron, D. J. *J. Am. Chem. Soc.* **2015**, *137*, 9160−9166.
(15) Liu, B.; Chen, H. M.; Liu, C.; Andrews, S. C.; Hahn, C.; Yang, P. D. *J. Am. Chem. Soc.* **2013**, *135*, 9995−9998.
(16) Lu, X. J.; Yang, W. G.; Quan, Z. W.; Lin, T. Q.; Bai, L. G.; Wang, L.; Huang, F. Q.; Zhao, Y. S. *J. Am. Chem. Soc.* **2014**, *136*, 419−426.
(17) Yang, C. Y.; Wang, Z.; Lin, T. Q.; Yin, H.; Lu, X. J.; Wan, D. Y.; Xu, T.; Zheng, C.; Lin, J. H.; Huang, F. Q.; Xie, X. M.; Jiang, M. H. *J. Am. Chem. Soc.* **2013**, *135*, 17831−17838.
(18) Feng, N. D.; Wang, Q.; Zheng, A. M.; Zhang, Z. F.; Fan, J.; Liu, S. B.; Amoureux, J. P.; Deng, F. *J. Am. Chem. Soc.* **2013**, *135*, 1607−1616.
(19) Chen, X.; Mao, S. S. *Chem. Rev.* **2007**, *107*, 2891−2959.
(20) Khan, S. U. M.; Al-Shahry, M.; Ingler, W. B., Jr *Science* **2002**, *297*, 2243−2245.
(21) Park, J. H.; Kim, S.; Bard, A. J. *Nano Lett.* **2006**, *6*, 24−28.
(22) Schneider, J.; Matsuoka, M.; Takeuchi, M.; Zhang, J. L.; Horiuchi, Y.; Anpo, M.; Bahnemann, D. W. *Chem. Rev.* **2014**, *114*, 9919−9986.
(23) Batzill, M.; Morales, E. H.; Diebold, U. *Phys. Rev. Lett.* **2006**, *96*, 026103.
(24) Zhu, W. G.; Qiu, X. F.; Iancu, V.; Chen, X. Q.; Pan, H.; Wang, W.; Dimitrijevic, N. M.; Rajh, T.; Meyer, H. M.; Paranthaman, M. P.; Stocks, G. M.; Weitering, H. H.; Gu, B. H.; Eres, G.; Zhang, Z. Y. *Phys. Rev. Lett.* **2009**, *103*, 226401.
(25) Gai, Y.; Li, J.; Li, S.-S.; Xia, J.-b.; Wei, S.-H. *Phys. Rev. Lett.* **2009**, *102*, 036402.
(26) Yin, W. J.; Wei, S. H.; Al-Jassim, M. M.; Yan, Y. F. *Phys. Rev. Lett.* **2011**, *106*, 066801.
(27) Hoang, S.; Berglund, S. P.; Hahn, N. T.; Bard, A. J.; Mullins, C. B. *J. Am. Chem. Soc.* **2012**, *134*, 3659−3662.
(28) Xu, W.; Jain, P. K.; Beberwyck, B. J.; Alivisatos, A. P. *J. Am. Chem. Soc.* **2012**, *134*, 3946−3949.
(29) George, S.; Pokhrel, S.; Ji, Z. X.; Henderson, B. L.; Xia, T.; Li, L. J.; Zink, J. I.; Nel, A. E.; Madler, L. *J. Am. Chem. Soc.* **2011**, *133*, 11270−11278.
(30) Zuo, F.; Wang, L.; Wu, T.; Zhang, Z. Y.; Borchardt, D.; Feng, P. Y. *J. Am. Chem. Soc.* **2010**, *132*, 11856−11857.
(31) Wang, S. B.; Pan, L.; Song, J. J.; Mi, W. B.; Zou, J. J.; Wang, L.; Zhang, X. W. *J. Am. Chem. Soc.* **2015**, *137*, 2975−2983.




DOI: 10.1021/acs.nanolett.7b03933
*Nano Lett.* 2018, 18, 1592−1599

(32) Li, Y. F.; Liu, Z. P.; Liu, L. L.; Gao, W. G. *J. Am. Chem. Soc.* **2010**, *132*, 13008−13015.
(33) Choi, W. Y.; Termin, A.; Hoffmann, M. R. *J. Phys. Chem.* **1994**, *98*, 13669−13679.
(34) Irie, H.; Watanabe, Y.; Hashimoto, K. *J. Phys. Chem. B* **2003**, *107*, 5483−5486.
(35) Shulman, R. G.; Wyluda, B. J. *Phys. Rev.* **1956**, *102*, 1455−1457.
(36) Collins, C. B.; Carlson, R. O.; Gallagher, C. J. *Phys. Rev.* **1957**, *105*, 1168−1173.
(37) Shockley, W.; Read, W. T. *Phys. Rev.* **1952**, *87*, 835−842.
(38) Di Valentin, C.; Pacchioni, G.; Selloni, A. *Phys. Rev. B: Condens. Matter Mater. Phys.* **2004**, *70*, 085116.
(39) Weng, H. M.; Yang, X. P.; Dong, J. M.; Mizuseki, H.; Kawasaki, M.; Kawazoe, Y. *Phys. Rev. B: Condens. Matter Mater. Phys.* **2004**, *69*, 125219.
(40) Long, R.; English, N. J. *Phys. Rev. B: Condens. Matter Mater. Phys.* **2011**, *83*, 2604−2608.
(41) Celik, V.; Mete, E. *Phys. Rev. B: Condens. Matter Mater. Phys.* **2012**, *86*, 205112.
(42) Cheney, C. P.; Vilmercati, P.; Martin, E.; Chiodi, M.; Gavioli, L.; Regmi, M.; Eres, G.; Callcott, T.; Weitering, H. H.; Mannella, N. *Phys. Rev. Lett.* **2014**, *112*, 036404.
(43) Yamamoto, T.; Ohno, T. *Phys. Rev. B: Condens. Matter Mater. Phys.* **2012**, *85*, 033104.
(44) McDonnell, K. A.; English, N. J.; Rahman, M.; Dowling, D. P. *Phys. Rev. B: Condens. Matter Mater. Phys.* **2012**, *86*, 115306.
(45) Tsetseris, L. *Phys. Rev. B: Condens. Matter Mater. Phys.* **2011**, *84*, 165201.
(46) Duncan, W. R.; Prezhdo, O. V. *Annu. Rev. Phys. Chem.* **2007**, *58*, 143−184.
(47) Zheng, Q.; Zhao, J. Hefei NAMD. http://staff.ustc.edu.cn/~zhaojin/code.html (accessed Oct. 24, 2016).
(48) Stroppa, A.; Kresse, G. *New J. Phys.* **2008**, *10*, 063020.
(49) Kresse, G.; Hafner, J. *Phys. Rev. B: Condens. Matter Mater. Phys.* **1993**, *48*, 13115−13118.
(50) Kresse, G.; Hafner, J. *Phys. Rev. B: Condens. Matter Mater. Phys.* **1994**, *49*, 14251−14269.
(51) Akimov, A. V.; Prezhdo, O. V. *J. Chem. Theory Comput.* **2014**, *10*, 789−804.
(52) Akimov, A. V.; Prezhdo, O. V. *J. Chem. Theory Comput.* **2013**, *9*, 4959−4972.
(53) Chu, W. B.; Saidi, W. A.; Zheng, Q. J.; Xie, Y.; Lan, Z. G.; Prezhdo, O. V.; Petek, H.; Zhao, J. *J. Am. Chem. Soc.* **2016**, *138*, 13740−13749.
(54) Perdew, J. P.; Burke, K.; Ernzerhof, M. *Phys. Rev. Lett.* **1996**, *77*, 3865−3868.
(55) Blöchl, P. E. *Phys. Rev. B: Condens. Matter Mater. Phys.* **1994**, *50*, 17953−17979.
(56) Tully, J. C. *Classical and Quantum Dynamics in Condensed Phase Simulations*; World Scientific: Singapore, 1998.
(57) De Sio, A.; Troiani, F.; Maiuri, M.; Rehault, J.; Sommer, E.; Lim, J.; Huelga, S. F.; Plenio, M. B.; Rozzi, C. A.; Cerullo, G.; Molinari, E.; Lienau, C. *Nat. Commun.* **2016**, *7*, 13742.
(58) Nijamudheen, A.; Akimov, A. V. *J. Phys. Chem. C* **2017**, *121*, 6520−6532.
(59) Ozawa, K.; Emori, M.; Yamamoto, S.; Yukawa, R.; Yamamoto, S.; Hobara, R.; Fujikawa, K.; Sakama, H.; Matsuda, I. *J. Phys. Chem. Lett.* **2014**, *5*, 1953−1957.
(60) Xu, M. C.; Gao, Y. K.; Moreno, E. M.; Kunst, M.; Muhler, M.; Wang, Y. M.; Idriss, H.; Woll, C. *Phys. Rev. Lett.* **2011**, *106*, 138302.
(61) Yamada, Y.; Kanemitsu, Y. *Appl. Phys. Lett.* **2012**, *101*, 133907.
(62) Furube, A.; Asahi, T.; Masuhara, H.; Yamashita, H.; Anpo, M. *J. Phys. Chem. B* **1999**, *103*, 3120−3127.
(63) Bahnemann, D. W.; Hilgendorff, M.; Memming, R. *J. Phys. Chem. B* **1997**, *101*, 4265−4275.
(64) Fujihara, K.; Izumi, S.; Ohno, T.; Matsumura, M. *J. Photochem. Photobiol., A* **2000**, *132*, 99−104.
(65) Kazempour, A. *Phys. Scr.* **2015**, *90*, 025804.
(66) Reeves, K. G.; Schleife, A.; Correa, A. A.; Kanai, Y. *Nano Lett.* **2015**, *15*, 6429−6433.
(67) Shakouri, A., Recent Developments in Semiconductor Thermoelectric Physics and Materials. In *Annual Review of Materials Research*, Clarke, D. R.; Fratzl, P., Eds. Annual Reviews: Palo Alto, 2011; Vol. *41*, pp 399−431.
(68) Holland, M. G. *Phys. Rev.* **1964**, *134*, A471−480.
(69) Estreicher, S. K.; Gibbons, T. M.; Kang, B.; Bebek, M. B. *J. Appl. Phys.* **2014**, *115*, 012012.
(70) Jaiswal, R.; Patel, N.; Dashora, A.; Fernandes, R.; Yadav, M.; Edla, R.; Varma, R. S.; Kothari, D. C.; Ahuja, B. L.; Miotello, A. *Appl. Catal., B* **2016**, *183*, 242−253.
(71) El Koura, Z.; Patel, N.; Edla, R.; Miotello, A. *Int. J. Nanotechnol.* **2014**, *11*, 1017−1027.
(72) Zhang, M.; Lu, D. D.; Zhang, Z. H.; Yang, J. J. *J. Electrochem. Soc.* **2014**, *161*, H416−H421.
(73) Zhang, M.; Lu, D. D.; Zhang, Z. H.; Guo, Y. R.; Yang, J. J. *J. Electrochem. Soc.* **2015**, *162*, H557−H563.
(74) Patel, N.; Jaiswal, R.; Warang, T.; Scarduelli, G.; Dashora, A.; Ahuja, B. L.; Kothari, D. C.; Miotello, A. *Appl. Catal., B* **2014**, *150*, 74−81.
(75) Liu, J. W.; Han, R.; Zhao, Y.; Wang, H. T.; Lu, W. J.; Yu, T. F.; Zhang, Y. X. *J. Phys. Chem. C* **2011**, *115*, 4507−4515.



DOI: 10.1021/acs.nanolett.7b03933
*Nano Lett.* 2018, 18, 1592−1599